

Surface Winds and Energy Fluxes Near the Greenland Ice Margin under Conditions of Katabatic Winds

by Günther Heinemann¹ and Ulrike Falk²

Summary: Surface winds and energy fluxes from measurements of stations on the ice sheet and in the tundra area near Kangerlussuaq, West Greenland, are presented for the period of the experiment KABEG (Katabatic wind and boundary layer front experiment around Greenland) in April/May 1997. For almost all days a nighttime development of the katabatic wind is found over the ice sheet causing a peak to peak amplitude of up to 5 m/s for the wind speed anomaly. A variational approach is used to compute turbulent fluxes from profiles in the surface layer over the ice sheet and over the tundra area. The fluxes over the tundra area are validated using direct eddy-correlation flux measurements. Profile-derived sensible heat fluxes show the tendency to overestimate the absolute flux values for stable conditions over the tundra area. Nighttime conditions over the tundra are also found to be associated with intermittent turbulence and instationarity. In contrast, katabatic wind conditions over the ice sheet are associated with continuous turbulence and quasi-stationary profiles. The energy loss by the net radiation over the ice sheet is compensated to a large extent by the turbulent flux of sensible heat during strong wind conditions. Mean roughness lengths for neutral conditions show values of 2.3 cm and 1.1×10^{-4} m for the vegetated tundra area and the ice surface, respectively.

Zusammenfassung: Es werden Wind- und Energiebilanzmessungen im Bereich des grönländischen Eisrandes präsentiert, die mit Hilfe von Stationen auf dem Eisschild und in der Tundra nahe Kangerlussuaq (West-Grönland) während des Zeitraums des Experiments KABEG (Katabatic wind and boundary layer front experiment around Greenland) im April/Mai 1997 gewonnen wurden. An fast allen Tagen wird die nächtliche Entwicklung des katabatischen Windes über dem Eisschild beobachtet, die mit einer Amplitude von bis zu 5 m/s in der Windgeschwindigkeitsanomalie verbunden ist. Ein Variationsansatz wird zur Berechnung der turbulenten Flussdichten aus Profilmessungen in der Prandtl-Schicht über dem Eisschild und im Bereich der Tundra verwendet. Die Flussdichten über der Tundra werden mit direkten Eddy-Korrelationsmessungen validiert. Die aus den Profilen abgeleiteten Flussdichten sensibler Wärme zeigen über der Tundra eine Tendenz zur starken Überschätzung des absoluten Wertes der Flussdichten für stabile Schichtung während der Nacht. Diese Bedingungen sind auch verbunden mit intermittierender Turbulenz und Instationarität. Im Unterschied dazu sind die Verhältnisse in der durch den katabatischen Wind geprägten Prandtl-Schicht über dem Eisschild mit kontinuierlicher Turbulenz und quasi-stationären Profilen verbunden. Der Energieverlust durch die Strahlungsbilanz über dem Eisschild wird bei starkem katabatischen Wind zum großen Teil durch die Flussdichte sensibler Wärme kompensiert. Die Bestimmung von Rauigkeitslängen für neutrale Schichtung ergibt mittlere Werte von 2,3 cm für die Tundra und $1,1 \times 10^{-4}$ m für die Oberfläche des Inlandeises.

INTRODUCTION

The ice sheet of Greenland covers an area of 1.75×10^6 km², and the air/snow energy and momentum exchange at its surface represents a key factor for the near-surface climate. A stable stratification over the ice slopes leads to the development of the katabatic wind system. The Greenland ice margin generally reveals a topographic gradient exceeding 1 % over large areas (Fig. 1), and associated katabatic winds are observed

with speeds up to gale force (PUTNINS 1970, RASMUSSEN 1989). Air/snow interaction processes are enhanced during katabatic wind situations, and therefore the knowledge of katabatic flow characteristics and associated air/snow exchange processes are important for questions of the mass balance of the ice sheet. For example, OHMURA et al. (1996) found for climate simulations with doubled CO₂ that the main change in the snow accumulation (precipitation minus evaporation) of the Greenland ice sheet would occur in form of an increased surface flux of latent heat, and that a change in the surface energy balance components would lead to a drastically increased ablation.

During the last ten years, two major efforts for the investigation of the surface energy balance and the boundary layer over Greenland were made. The first major effort was the Greenland Ice Margin Experiment (GIMEX, OERLEMANS & VUGTS 1993) in combination with the ETH Greenland Expedition (1990-1993). Direct eddy-correlation flux measurements were made at various heights up to 30 m over the ice sheet (FORRER & ROTACH 1997, FORRER 1999, MEESTERS et al. 1997). The second major effort was the experiment KABEG (Katabatic wind and boundary layer front experiment around Greenland) in April/May 1997 in the area of southern Greenland (HEINEMANN 1998, 1999). For the first time, aircraft-based direct turbulence measurements were performed in the whole boundary layer over the ice sheet. In addition, surface stations were installed at five positions in the tundra and over the ice sheet during KABEG, in order to determine surface energy balance components and a horizontal profile of the wind field structure.

First results of KABEG are presented in HEINEMANN (1999). Vertical profiles flown by the aircraft showed boundary layer heights over the ice slope between 70 and 200 m, and low-level jets (LLJs) with wind speeds of up to 25 m/s. Studies of the boundary layer dynamics yielded the result that the katabatic force is the main driving mechanism for the flow regime over the ice sheet. Mesoscale model simulations for katabatic winds during KABEG and comparisons with aircraft and surface data (KABEG and AWS measurements of the PARCA program, STEFFEN et al. 1996) have been performed by KLEIN et al. (2001a,b).

The main goal of the present study is to present results of the KABEG surface stations, particularly the evaluation of surface fluxes near the ice margin. The paper is structured as follows: A first section describes the experimental area, the stations and evaluation methods. Details of the variational method are given in Appendices I and II. In the result section, two case studies are presented with strong and weak synoptic forcing,

¹ Meteorologisches Institut der Universität Bonn, Auf dem Hügel 20, D-53121 Bonn, Germany; <gheinemann@uni-bonn.de>

² Institut für Bioklimatologie der Universität Göttingen

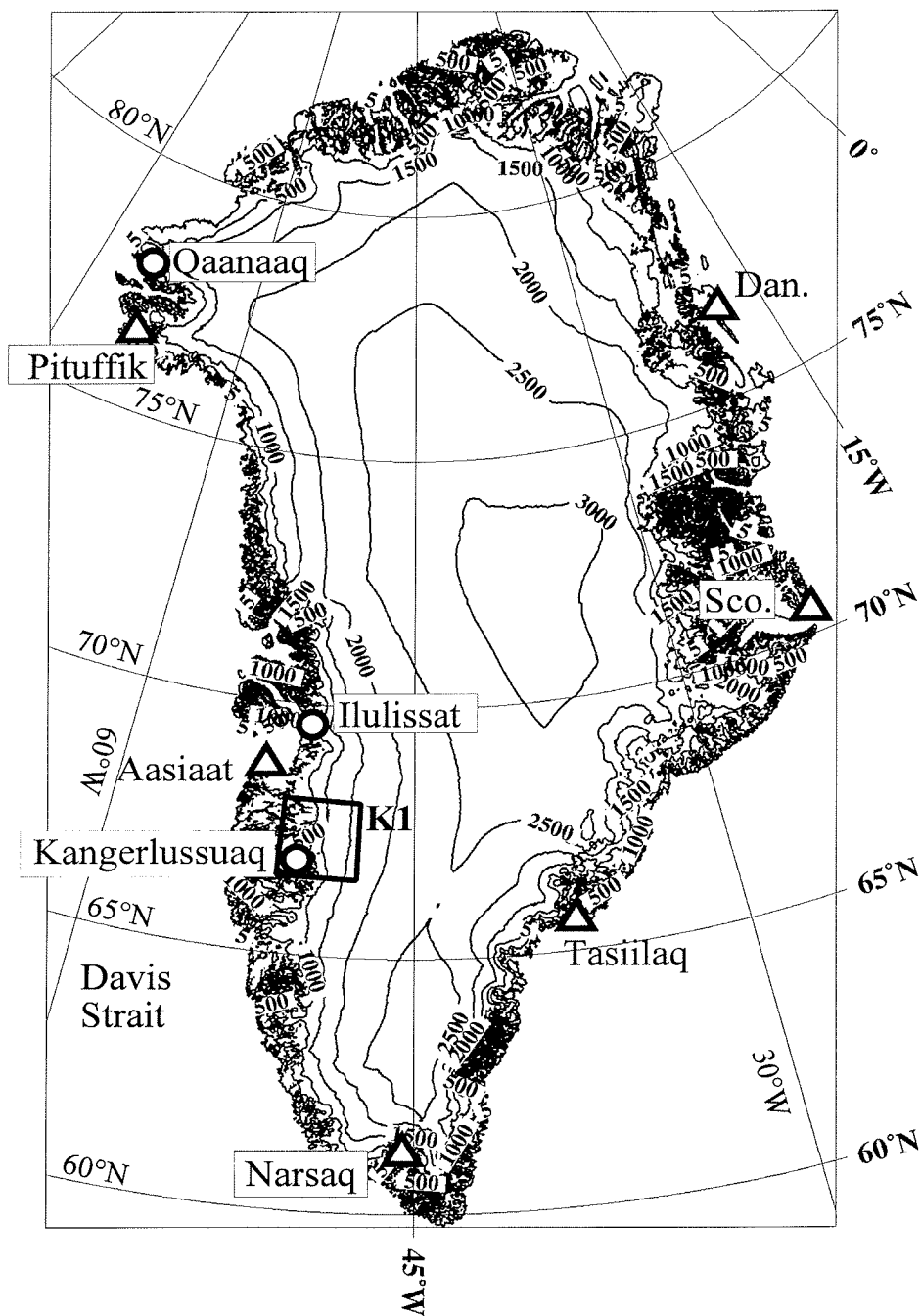


Fig. 1: Map of Greenland with topography (isolines every 500 m) from high resolution (2 km) topography data (EKHOLM 1996). Triangles mark the radiosonde stations. The box K1 indicates the area shown in Fig. 2.

Abb. 1: Karte von Grönland mit Orographie (Isolinienabstand 500 m) aus hochaufgelösten Orographie-Daten nach EKHOLM (1996). Dreiecke markieren Radiosondenstationen; die Box K1 markiert das Gebiet, das in Abb. 2 gezeigt wird.

respectively, followed by statistics covering the whole KABEG period. Summary and conclusions are given in the last Section.

EXPERIMENT SETUP, DATA AND METHODS

Experimental area and data

The base of the KABEG experiment was Kangerlussuaq (former Søndre Strømfjord, West Greenland, Fig. 1) at a distance of about 20 km from the glaciers of the inland ice sheet. During the experiment, surface stations were installed at five positions (Fig. 2). The tundra area of West Greenland is a hilly terrain with tundra vegetation. Even the high-resolution topography data of EKHOLM (1996) with 2.2 km resolution shown

in Figure 2 is not able to resolve all relevant topographic details. The tundra area is characterized by big fjords, small lakes, and numerous small hills and valleys. Thus the aerodynamic roughness is largely increased over the tundra area, while it is very small for the ice sheet. The KABEG period (12 April to 15 May 1997) was characterized by a snow covered tundra area and frozen soil during the first two weeks. In contrast, a transition to almost summertime conditions took place at the beginning of May, and 2 m-temperature maxima near Kangerlussuaq were up to +15 °C (HEINEMANN 1999). However, non-melting conditions were still present for the major part of the ice sheet (maximum air temperatures above 0 °C were measured over the ice sheet at station A3 only on four days and never at A4; see Fig. 2 for locations).

KABEG area K1

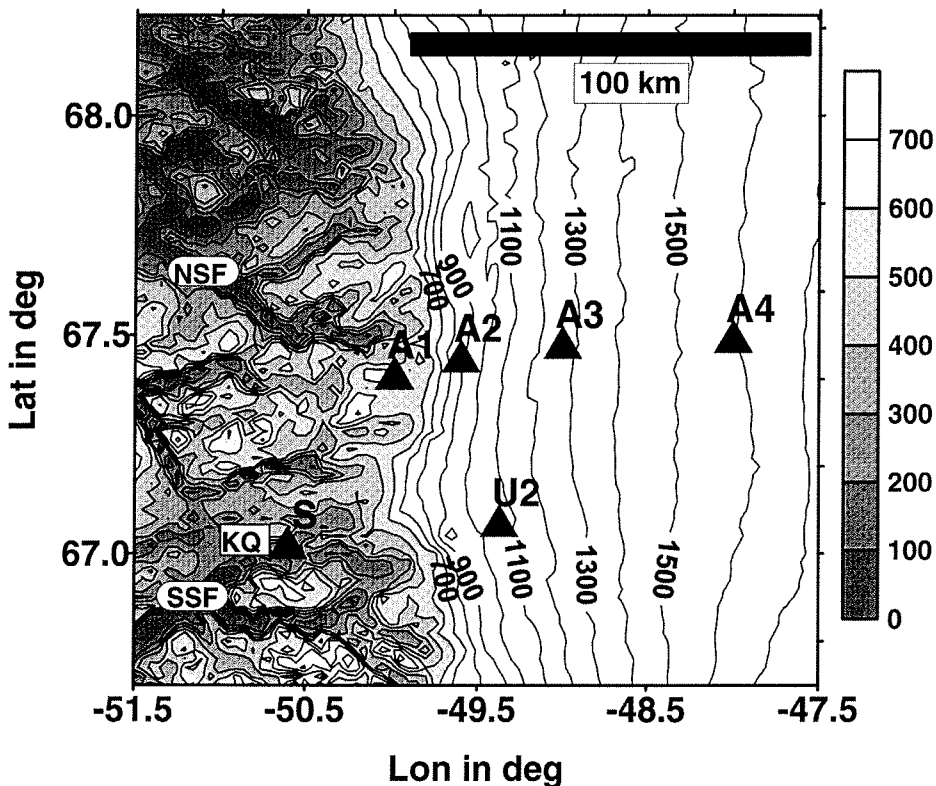


Fig. 2: Area of the KABEG experiment near Kangerlussuaq (box in Fig. 1) with a high-resolution (2 km) topography (EKHOLM 1996). Isolines are drawn every 100 m, areas lower than 700 m are shaded (see gray scale). The triangles mark the positions of the surface stations A1-A4, U2 and S (near Kangerlussuaq, KQ). SSF and NSF mark the fjord valleys Søndre Strømfjord and Nordre Strømfjord, respectively.

Abb. 2: Gebiet des KABEG-Experiments bei Kangerlussuaq (Box in Abb. 1) mit hochauflösender Orographie nach EKHOLM (1996). Der Isolinienabstand beträgt 100 m, Gebiete tiefer als 700 m sind schattiert (s. Grauskala). Dreiecke markieren die Positionen der Bodenstationen A1-A4, U2 und S (nahe Kangerlussuaq, KQ). SSF und NSF markieren die Fjord-Täler Søndre Strømfjord bzw. Nordre Strømfjord.

In the fjord valley near Kangerlussuaq (at position S in the Sandflugtdalen, 40 m ASL; see Fig. 2) a station with eddy-correlation turbulent heat flux and momentum measurements (3D sonic anemometer/thermometer at 3.3 m, Metek USA-1, data sampled at 20 Hz) was installed. About 200 hours of eddy-correlation data were collected on 16 days during the period 15 April to 14 May 1997. At the same position (Fig. 3a) surface layer profiles of air temperature, humidity and wind speed were measured at five levels (electrically ventilated PT100 (MIUB) and cup anemometers (Vector Instr.) at 0.5, 0.8, 1.1, 1.7 and 2.6 m), wind direction at 3.2 m (wind vane, Vector Instr.), net radiation at 1.4 m (net pyrradiometer, Thies), air pressure (piezoresistive pressure sensor, Honeywell), and the soil temperature profile (using PT100 (MIUB) at depths of -0.02, -0.05, -0.1, -0.2, -0.5 m). The measurements allow to determine the surface energy balance components. Station S was built up in order to represent the flow characteristics and the energy balance in a large fjord valley of the tundra area. The tundra vegetation at S in the fjord valley had a height of about 0.5 m (see Fig. 3a). The determination of turbulent surface fluxes from the profile measurements (see result section) is limited by the spatial inhomogeneities of the surface characteristics. Besides the influences of the profile mast and the mast of the eddy-correlation measurements on the profiles, the closeness of the valley mountains and a (frozen) river restricted the usable wind directions for the evaluation of profile measurements. A sufficient fetch and undisturbed conditions were only present for three sectors of the wind direction (30-140°, 180-230°, 270-330°).

Along a line orientated parallel to the fall line at about 50 km north of Kangerlussuaq four stations were installed (Fig. 2):

two wind recorders A1 and A2 over the tundra area close to the edge of the inland ice (at a distance of 12 km to the ice edge, 600 m ASL) and over the inland ice close to the ice edge (5 km, 760 m ASL); and two surface energy balance stations over the ice at distances of about 30 km (A3, 1200 m ASL) and 75 km (A4, 1600 m ASL) from the ice edge. A detailed description of the instrumentation is given in HEINEMANN (1999). Station A4, being furthest from the ice edge, is taken as the main energy balance station over the ice sheet in this study (Fig. 3b). The measurements comprised air temperature and wind speed using electrically ventilated PT100 (MIUB) and cup anemometers (Vector Instr.) at three levels (0.3, 0.8, 1.9 m), wind direction at 2.4 m (wind vane, Vector Instr.), net radiation at 1.4 m (net pyrradiometer, Thies), snow temperatures using PT100 (MIUB) at five depths (-0.2, -0.25, -0.3, -0.4, -0.7-m) and air pressure (piezoresistive pressure sensor, Honeywell). Snow accumulation over the ice sheet was about 0.2 m over the KABEG period. Energy for the ventilation and the instruments was supplied by solar panels, and data were recorded as 15 min means.

In addition to the KABEG stations, data from an automatic weather station on the ice sheet operated by the University of Utrecht (IMAU) is available in the KABEG area (marked as U2 in Fig. 2 at 67.0764 °N/49.3714 °W, 1015 m ASL).

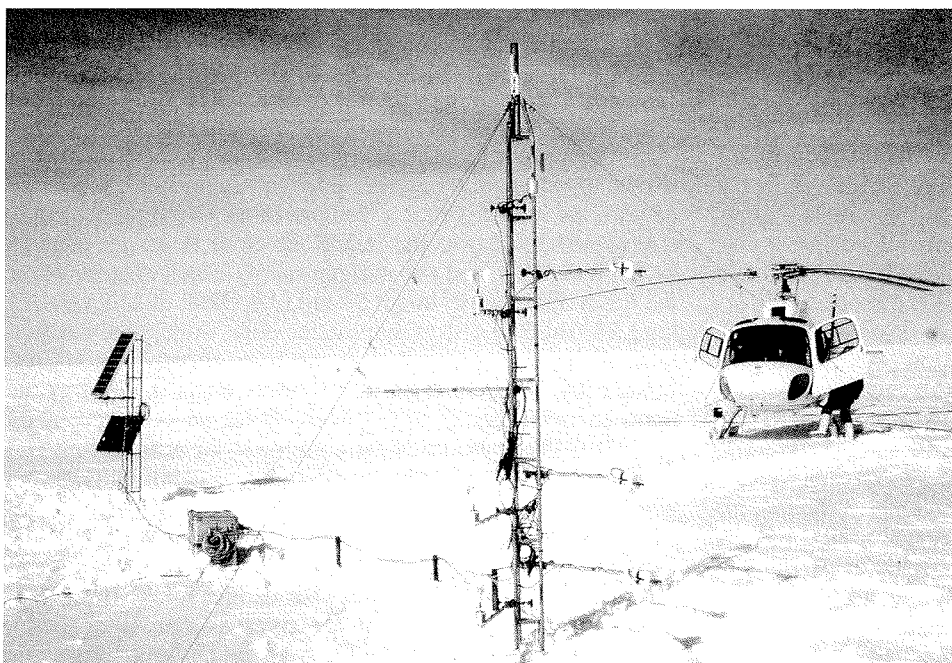


Fig. 3: (a, top) Surface station S (profile measurements) in the tundra area near Kangerlussuaq in May 1997. The booms of the anemometers are orientated approximately parallel to the valley axis (inland ice to the right). (b, bottom) Surface station A4 on the ice sheet in April 1997 (details see text).

Abb. 3: (a, oben) Station S (Profilmessungen) in der Tundra nahe Kangerlussuaq im May 1997. Die Ausleger der Anemometer sind ungefähr parallel zur Talachse ausgerichtet (Inlandeis rechts). (b, unten) Station A4 auf dem Eisschild im April 1997 (Details s. Text).

Data evaluation

Turbulence measurements

The 20 Hz turbulence measurements of the 3D wind vector and the temperature at station S in the fjord valley are used to obtain direct measurements of turbulent fluxes of momentum and sensible heat applying the eddy-covariance (EC) technique. A software package developed at the MIUB by SVENSSON (1997) was applied, which includes the rotation of the coordinate system in the mean wind direction, detrending, a check of the turbulence stationarity and integral length scales, computation of turbulent fluxes and similarity functions for

scaled variances and dissipation. The results shown are based on 30 or 60 min sampling periods. The stationarity check is performed by using five subintervals of the sampling period, and a deviation of the individual subsamples of turbulent fluxes from the average flux of less than 30 % is regarded as being stationary (FOKEN & WICHURA 1996).

Profile measurements

The well-known Bowen ratio energy balance method (BOWEN 1926) for the determination of turbulent energy fluxes cannot be applied for two reasons. Firstly, the gradients of the specific

humidity cannot be measured accurately enough with the available instrumentation for very low temperatures. Secondly, the determination of the soil heat flux in the tundra area was impossible because of melting and freezing of the soil, and because of the fact that the soil temperature sensors had not always good contact to the soil during the first phase of KABEG, when the soil was completely frozen. The snow heat flux at the energy balance stations over the ice sheet was computed by the heat storage method (see e.g. HEINEMANN & ROSE 1990), but the snow accumulation of about 0.2 m at the end of April 1997 caused large errors by using this method.

An alternative method was chosen based on the Monin-Obukhov (MO) similarity theory (MOST) using a variational approach. The method used follows the way outlined by XU and QUI (1997), a detailed description is given in Appendix I. A similar variational approach was used recently by MA and DAGGUPATY (2000), who added the transfer coefficient for heat (CH) as an additional constraint to the cost function shown in Eq. (I-1), in order to derive roughness lengths of heat and momentum.

Details about the method for the evaluation of the KABEG data are given in Appendix II. The cost function (J in (I-1)) is a measure of the closeness of the observed profiles to those of the MO similarity theory, and the absolute value of the gradient of the cost function (h in (I-4)) is a measure of the quality of the variational method in finding the minimum. Thus both values are taken as a quality control for the flux determination.

RESULTS

Case of strong synoptic forcing (22 April 1997)

The KABEG period represents springtime insolation conditions, and hence a pronounced daily cycle in the radiative forcing is present for small cloud coverage. The wind field near the ice margin is driven by local circulations caused by temperature contrasts between the boundary layer over the tundra area and the ice sheet, by katabatic forcing resulting from the cooling of the boundary layer over the ice sheet, and by synoptic forcing. Strong synoptic pressure gradients were present over the KABEG area during 21 and 22 April, leading to a period of strong winds over the ice sheet and well-developed low-level jets (HEINEMANN 1999). Numerical simulations by KLEIN et al. (2001a) show that a synoptic-scale low approaches the KABEG area during 21 April. This is also reflected by the AWS data in the KABEG area (not shown). A strong increase in wind speed occurs during the afternoon of 21 April being associated with an increase of the pressure differences between A4, U2 and S (see Fig. 2 for locations). In contrast to the situation of weak synoptic forcing shown below, winds decrease during the morning hours of 22 April, but are still relatively strong (around 10 m/s).

Figure 4a shows the horizontal structure of the katabatic wind from all AWS of the measurement line for 22 April 1997 (time in local solar time, LST). A1-A4 are indicated as stations 1-4. Since the topography gradient is in west-east direction (Fig. 2), an easterly wind is equivalent to a downslope wind. The downslope increase of the nighttime katabatic wind speed from A4 to A2 agrees with the increasing topography gradient

(0.7 % at A4, 1.1 % at A3, and 2 % at A2), and highest wind speeds over the ice sheet are found at A2. Also at A1 high winds are measured during the first hours of this day. While the wind direction is relatively homogeneous over the ice sheet, a distinct change in wind direction can be seen between A2 and A1. Station A1 was located in the tundra area at a distance of 12 km from the ice edge and on the top of a small hill. Apart from the channelling of the katabatic flow in the large fjord valleys like Søndre Strømfjord and Nordre Strømfjord (Fig.2), the extent of the katabatic flow over the tundra area was found to be about 10 km by aircraft measurements in a similar case study of strong synoptic forcing for 13 May 1997 by HEINEMANN (1999). Therefore, the wind regime at A1 is directly influenced by the downslope wind from the ice sheet under these conditions. The katabatic wind system does not establish again during the evening, which is a result of cloudiness prohibiting the cooling of the boundary layer (see below).

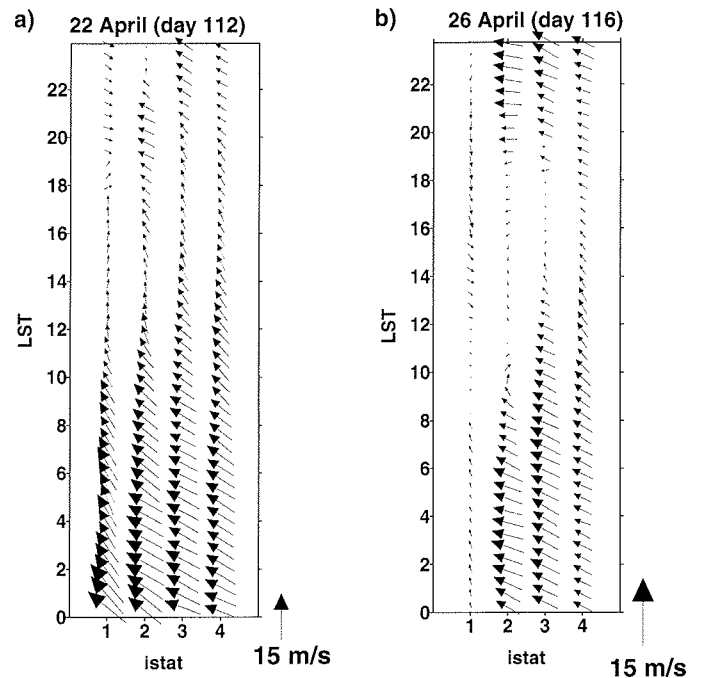
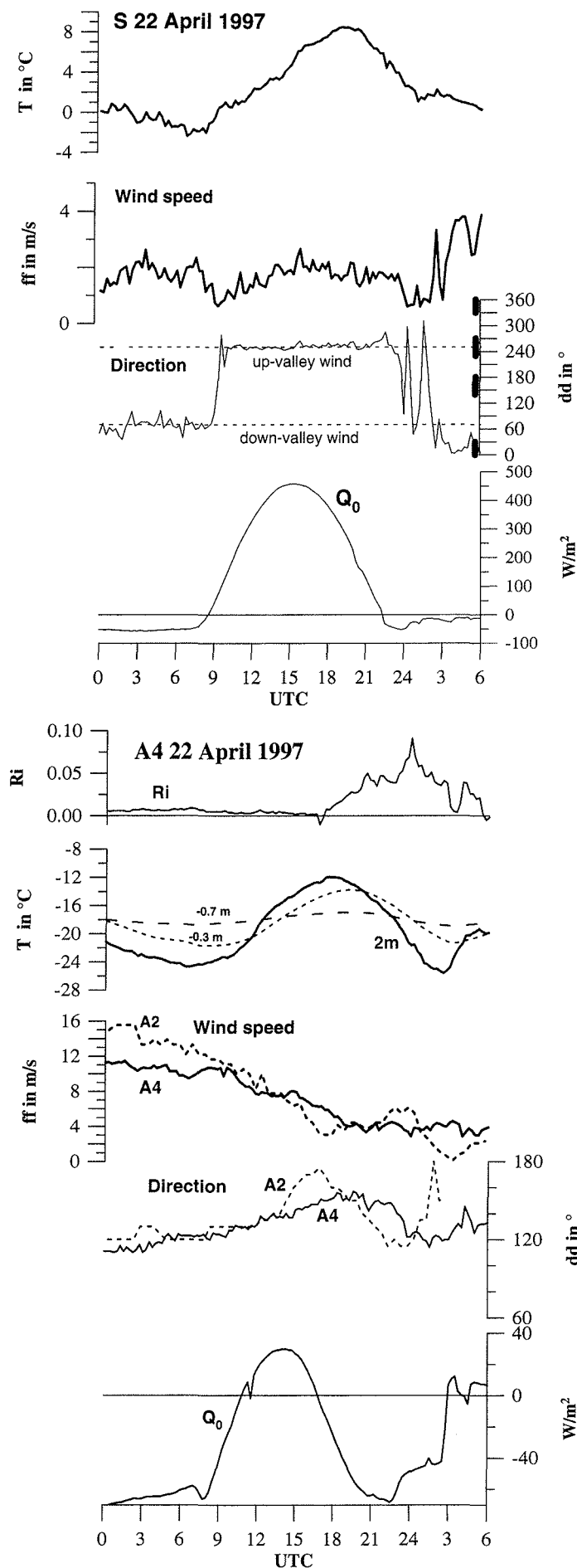


Fig. 4: Time series (LST is local solar time) of the wind vectors (every 30 min) at AWS of the KABEG measurement line for 22 April (part a) and 26 April 1997 (part b). The AWS A1-A4 are marked by istat = 1-4 (see Fig. 2). A scaling vector is shown at the lower right corner.

Abb. 4: Zeitreihe (LST ist die lokale Sonnenzeit) von Windvektoren (alle 30 min) an den AWS der KABEG-Messlinie für den 22. April (Teil a) und 26 April 1997 (Teil b). Die AWS A1-A4 sind mit istat = 1-4 gekennzeichnet (s. Abb. 2). Skalierungsvektor siehe untere rechte Ecke.

The situation in the fjord valley at station S near Kangerlussuaq for the period 00 UTC 22 April to 06 UTC 23 April is depicted in Figure 5a. The net radiation (Q_0) is negative during the night and reaches maximum values of about 500 W m^{-2} during daytime (note the time lag between UTC and local solar time (LST), i.e. noon is at about 15 UTC). The corresponding daily course of the temperature varies between -2 and $+9 \text{ }^\circ\text{C}$. During the first hours of 22 April, the wind direction is parallel to the valley axis in the sense of a down-valley wind, which represents a signal of the channelling of the katabatic flow as also found in high-resolution simulations by



KLEIN et al. (2001b). Around 9 UTC (6 LST) the wind direction changes by 180° to a up-valley wind and is almost constant the rest of the day. This change in flow direction in the fjord valley is mainly caused by the synoptic driven flow above the fjord valley. Although an effect of a possible valley wind system during daytime cannot be ruled out, it turns out to be of secondary importance, since an up-valley wind was not found to be typical for cloudless situations without synoptic forcing. The winds in the fjord valley are very weak and do hardly exceed 2 m/s on 22 April.

Completely different conditions were observed over the inland ice (Fig. 5b). The net radiation at station A4 also reveals a clear daily cycle, but is negative in the daily mean. Maximum values are around $+30 \text{ W m}^{-2}$ only. The daily course of the temperature is also pronounced. The daily temperature cycle can also be seen in the snow temperature at -0.3 m , while temperatures at -0.7 m are almost constant. The phase lag between the net radiation and the temperature is evident. Net radiation drops down to negative values during the evening, but then clouds prohibit further cooling and lead to a temperature increase and positive values for the net radiation during the first hours of 23 April. Consequently, the development of the nighttime katabatic flow is suppressed during the morning of 23 April (Fig. 4a). Wind speeds are up to 16 m/s at A2 during the morning of 22 April, and with decreasing synoptic and katabatic forcing wind speeds drop to 4 m/s at A2 and A4. Richardson numbers (computed from gradients between 1.9 and 0.3 m) are quite small (but positive) during the strong wind conditions, but the cooling phase during the afternoon is associated with relative large values of the Richardson number. While the course of the wind speed is strongly influenced by the synoptic forcing, the katabatic signal is still present in the wind direction, which is around 120° for katabatic flow directions.

The sensible heat flux H_0 and the net radiation Q_0 for the tundra station S for 22 April is displayed in Figure 6a. HSP denotes H_0 calculated from the variational analysis. HSP com-

Fig. 5: Time series of selected quantities (15 min averages) at stations S near Kangerlussuaq and A4 on the inland ice for 00 UTC 22 April to 06 UTC 23 April.

Part a: Station S; upper panel: temperature at 2.7 m; second panel: wind speed at 2.6 m; third panel: wind direction (thin line) at 3.2 m, dashed lines mark the directions parallel to the fjord valley axis, sectors with insufficient fetch are indicated as black bars; lower panel: net radiation.

Part b: Station A4; upper panel: gradient Richardson number; second panel: temperature at 1.9 m (thick line), snow temperatures at -0.3 and -0.7 m (dashed lines); third panel: wind speed at 1.9 m (thick solid line); fourth panel: wind direction (thin solid line) at 2.4 m; lower panel: net radiation. In addition, 2 m wind speed and direction at station A2 are shown as dashed lines.

Abb. 5: Zeitreihen ausgewählter Größen (15 min-Mittel) an den Stationen S nahe Kangerlussuaq und A4 auf dem Inlandeis für 00 UTC, 22. April, bis 06 UTC, 23. April.

Teil a: Station S; oberes Teilbild: Temperatur in 2.7 m; zweites Teilbild: Windgeschwindigkeit in 2.6 m; drittes Teilbild: Windrichtung (dünne Linie) in 3.2 m, gestrichelte Linien markieren Richtungen parallel zur Achse des Fjord-Tals, Sektoren mit unzureichender Anströmstrecke sind mit schwarzen Balken gekennzeichnet; unteres Teilbild: Strahlungsbilanz.

Teil b: Station A4; oberes Teilbild: Gradient-Richardsonzahl; zweites Teilbild: Temperatur in 1.9 m (dicke Linie), Firntemperaturen in -0.3 und -0.7 m (gestrichelte Linien); drittes Teilbild: Windgeschwindigkeit in 1.9 m (dicke durchgezogene Linie); viertes Teilbild: Windrichtung (dünne durchgezogene Linie) in 2.4 m; unteres Teilbild: Strahlungsbilanz. Zusätzlich sind die 2 m-Windgeschwindigkeit und Windrichtung an der Station A2 als gestrichelte Linien dargestellt.

compensates the negative Q_0 of about -50 W m^{-2} during the night almost completely. Since the latent heat flux E_0 can be assumed to be very small for temperatures below $0 \text{ }^\circ\text{C}$, this means that the soil heat flux B_0 is also small for the frozen ground with temperatures around $-6 \text{ }^\circ\text{C}$ during nighttime. HSP has values around 200 W m^{-2} during noon and compensates 30-50 % of the radiational energy input. But, as discussed in Appendix II, large errors are found for HSP during daytime. The error bars result from the differences between the measured profiles and profiles according to MO similarity. A likely reason for these large differences is the insufficient fetch for the up-valley wind direction (Fig. 5a). The sensible heat flux calculated from the sonic measurements (HEC) is shown for comparison. While HSP and HEC agree with the errors given by the variational method during daytime, HEC is close to zero during nighttime, and HSP is much more negative. This difference is also reflected in the stability parameter z/L_* , which is calculated for heights of 2.0 and 3.3 m for the profile and eddy-correlation measurements, respectively. Both, HEC and HSP seem to be not reliable during nighttime weak wind conditions in the fjord valley on 22 April. Wind speeds are between 1 and 2 m/s only (Fig. 5a), and the turbulence data on 22 April show periods of intermittent turbulence as well as gravity waves during nighttime (not displayed). Thus, fluxes computed by the standard EC method are not reliable for these conditions. At the same time, the surface layer profiles are highly instationary during nighttime, which is a severe restriction to the application of the MO similarity. It can also

be suspected that the height of the surface layer might be very low, and that the constant flux layer may be too thin for the measurement setup. On the other hand, it is not advisable to perform turbulence measurements closer to the ground, since the size of the turbulence elements should be large enough to be captured by the sonic anemometer.

Over the ice sheet (Fig. 6b), the turbulent flux of sensible heat almost compensates the radiative loss by the negative net radiation during the strong katabatic winds between 00 and 08 UTC. The cooling of the upper snow layers (Fig. 5b) leads to a negative soil heat flux during that period. The residuum (Res = $Q_0 - H_0 - B_0$) is very small. The sensible heat flux stays negative also for the short period of positive net radiation, but errors are quite large. After 16 UTC, Q_0 gets negative again, but H_0 is only about -20 W m^{-2} under conditions of much weaker winds compared to the morning. The soil heat flux is around $\pm 20 \text{ W m}^{-2}$, and Res has about the same values as Q_0 during the cooling period in the afternoon. The likely reason for this large imbalance are errors in B_0 , since the latent heat flux can be assumed to be very small for temperatures around $-20 \text{ }^\circ\text{C}$. Apart from uncertainties in the snow parameters (the snow density profile was measured), the heat storage in the upper snow layer is not adequately accounted for. Unfortunately the actual snow height (or depths of the snow thermometers) was measured only three times during the KABEG period, and no radiometric surface temperature is available for the computation of B_0 . As it is shown in other studies (e.g.

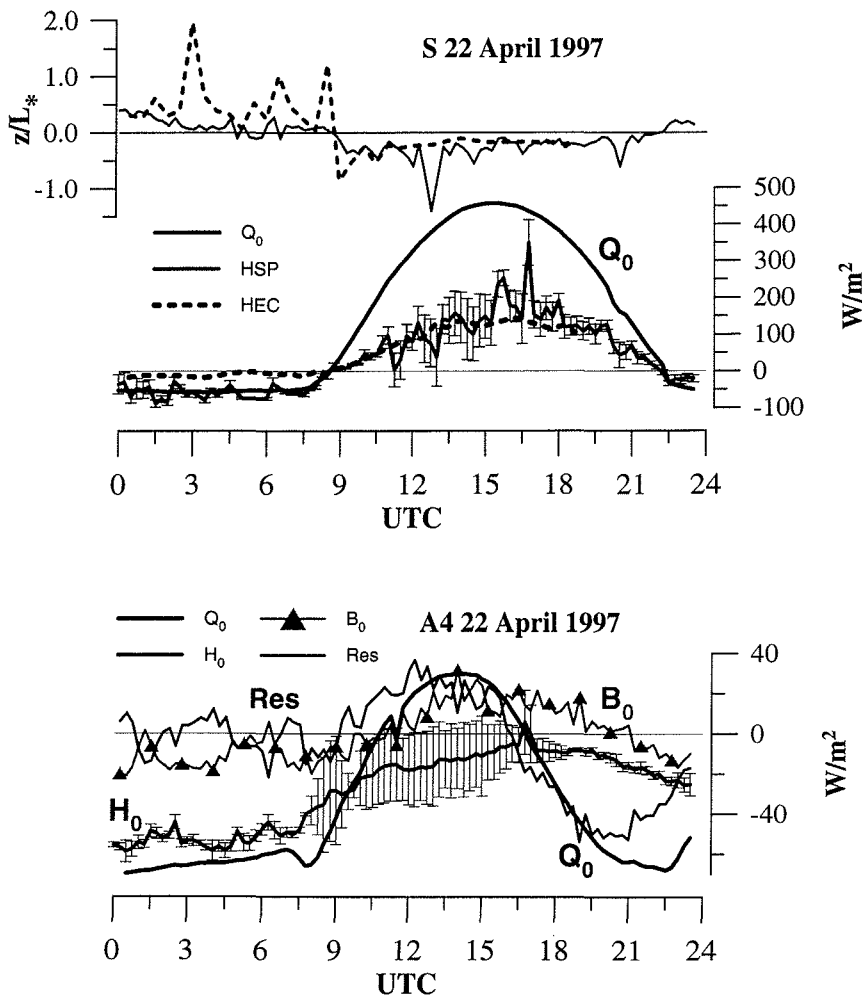


Fig. 6: Daily course of the energy balance components for 22 April at S (part a, top) and at A4 (part b, bottom). In part a, HSP denotes the sensible heat flux computed from the profile measurements (error bars as computed by the variational method), while HEC is the the sensible heat flux computed from the eddy correlation measurements. The stability parameter z/L_* is also shown for both methods for heights of 2 m (HSP) and 3.3 m (HEC). In part b, the residuum is defined as $\text{Res} = Q_0 - H_0 - B_0$.

Abb. 6: Tagesgang der Energiebilanz-Komponenten für den 22. April an S (Teil a, oben) und an A4 (Teil b, unten). In Teil a bedeutet HSP die Flussdichte sensibler Wärme berechnet aus den Profilmessungen (Fehlerbalken aus der variationellen Methode berechnet), während HEC die Flussdichte sensibler Wärme aus den Eddy-Korrelationsmessungen darstellt. Der Stabilitätsparameter z/L_* wird für Höhen von 2 m (HSP) bzw. 3.3 m (HEC) gezeigt. In Teil b wird das Residuum als $\text{Res} = Q_0 - H_0 - B_0$ definiert.

HEINEMANN & ROSE 1990), the heat storage in the upper few centimeters of the snow layer is responsible for a large fraction of B_0 .

Case of weak synoptic forcing (26 April 1997)

The day discussed in this section lies in a period of weak synoptic pressure gradients and almost cloudless conditions. Despite of temperatures being much lower, the daily course of the net radiation and the temperature in the fjord valley (not shown) is similar to that of 22 April. The main difference is found for the course of the wind direction. In contrast to 22 April, no change in the wind direction to an up-valley wind is present. Only low wind speeds (less than 4 m s^{-1}) and wind directions between 0° and 130° are found throughout the day.

The net radiation at station A4 (Fig. 7) also reveals a clear daily cycle with positive values only for 7 hours. The daily course of the 2 m-temperature is much more pronounced than in the tundra area (temperature ranges from -36°C to -17°C). In contrast to 22 April, a clear forcing of the net radiation on the daily course of the wind speed is present over the ice sheet. It should be noted that not the fluxes of net radiation and sensible heat, but only their divergences cause a cooling of the boundary layer, which results in a katabatic flow. The variation in wind speed between daytime and nighttime conditions is even more pronounced at station A2 lying closer to the ice edge and in an area of a larger topography gradient compared to A4 (Fig. 2). While wind speeds at A2 and A4 are around 7 and 5 m/s during nighttime (strong negative net radiation), they decrease to about 1 m/s (A2) and 2 m/s (A4) during daytime. Accordingly, the daily course of the wind direction reflects the

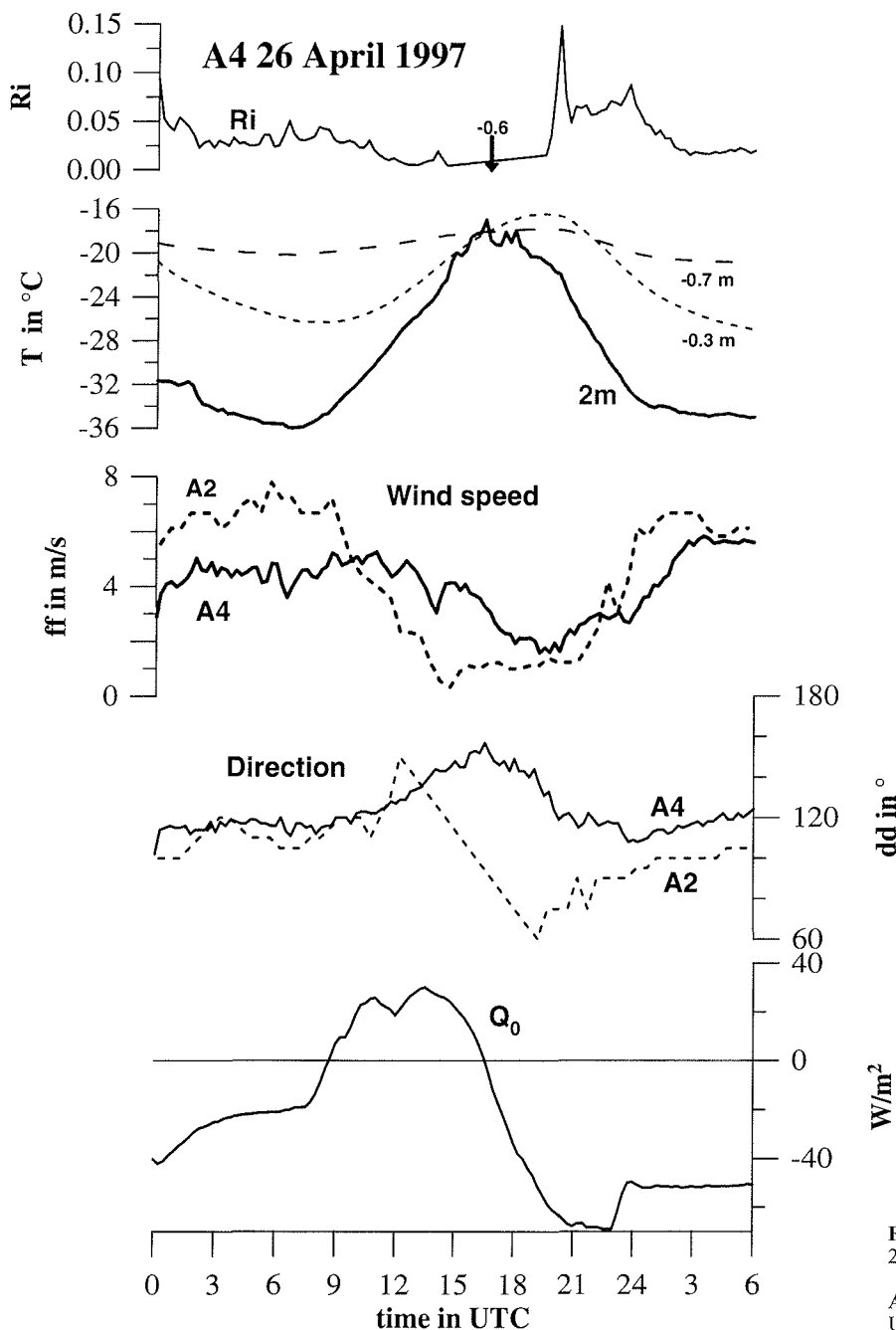


Fig. 7: As Figure 5b, but for 00 UTC 26 April to 06 UTC 27 April.

Abb. 7: Wie Abb. 5b, aber für 00 UTC, 26. April, bis 06 UTC, 27. April.

coupling between nighttime cooling and the development of the katabatic wind. During the cooling phase in the afternoon the wind turns from 150° to 120° at A4. Again the phase lag between the net radiation and the temperature is present, and the stabilization of the surface layer during the cooling phase is associated with relative large values of the Richardson number, which decrease afterwards with the increase of the nighttime katabatic wind.

The horizontal structure of the katabatic wind from all AWS of the measurement line for 26 April 1997 is shown in Figure 4b. A clear daily cycle can be seen for all stations on the ice sheet. Like for 22 April, the katabatic wind speed increases from A4 to A2 in agreement with the increasing topography gradient. In contrast to 22 April, the wind regime at A1 over the tundra area is not affected by the katabatic wind system. All stations over the ice sheet show only very weak winds during the afternoon. The onset of the katabatic wind occurs around 18 LST (sunset at about 20 LST), and the downslope wind system develops again over the ice sheet.

Turbulent surface fluxes of sensible heat are only shown for the ice sheet station A4, since fluxes computed for the tundra station showed large errors and eddy-correlation measurements are not available for 26 April. As shown in Appendix II, problems for the variational method for 26 April occur also for station A4, and results of good quality are obtained only between 00 and 14 UTC. Figure 8 displays Q_0 , H_0 and B_0 at A4 for 26 April (H_0 is not plotted for the period with the largest errors between 15 and 19 UTC). Like for 22 April, H_0 compensates Q_0 during nighttime. Absolute values of the fluxes are much smaller than on 22 April, but B_0 is of about the same magnitude. Since the latent heat flux can again be assumed to be negligible for temperatures down to -36°C , the main source of error for the surface energy balance can be seen in the heat storage in the upper snow layer, which is not measured by the experimental setup.

Statistics for the whole KABEG period (12 April - 15 May 1997)

Mean daily cycle for weak synoptic forcing

An overview over the mean daily cycle of the katabatic wind for weak synoptic forcing is displayed in Figure 9 for the period 26 April to 2 May 1997. In contrast to the simple averaging

of the data of the net radiation and wind direction, anomalies of temperature and wind speed have been calculated as deviations from low-pass filtered data (using a cut-off of 24 hours). This allows to exclude the influence of trends in the latter data, but preserves the daily cycles. The mean daily courses of net radiation and temperature anomaly at A4 is very similar to the case study shown in Figure 7, but amplitudes are reduced. The mean course of the wind speed anomaly shows significant differences between A2 and A4. At A4 the wind speed anomaly is relatively small, while the peak to peak amplitude is 5 m/s at A2. The decrease of the wind at A2 starts at about 8 LST (5 LST), and it is associated with a veering from wind directions of 120° (local fall line at A2 is 100°) to southerly wind directions during the afternoon. Nighttime wind directions at A4 are at an angle of about 45° relative to the fall line, which is typical for the fully developed katabatic wind over the homogeneous parts of the slope (KLEIN et al. 2001a), and indicate a balance between the katabatic force, Coriolis force and friction (HEINEMANN 1999).

Wind speed and direction distribution

The overall statistics of wind speed and direction distribution for the KABEG stations for the whole KABEG period are summarized in Figure 10 (data for A3 are not shown, since they are very similar to A4). For A4, a bimodal distribution is found for high windspeeds with one maximum for southerly directions (normal to the fall line, synoptic forcing) and the second for southeasterly directions (45° to the fall line, katabatic forcing). The katabatic wind peak is much more pronounced for A2, and highest wind speeds lie in the sector $90\text{-}130^\circ$ (local fall line is 100°). The wind speed distributions for the tundra area are quite different. A pronounced peak around 150° can be seen for A1, which can be interpreted as synoptically supported katabatic winds extending more than 10 km over the tundra area. In contrast to the stations over the ice sheet, a secondary maximum of northerly winds is found at A1. Only low wind speeds (less than 6 m s^{-1}) were recorded throughout the KABEG period at S. The distribution of the wind direction suggests the effects of the flow channelling and/or signals of a valley wind in the Kangerlussuaq fjord valley to be present.

Energy balance components

The calculations of the sensible heat flux H_0 and shear velocity u_* at A4 for the whole measurement period is shown in Figure

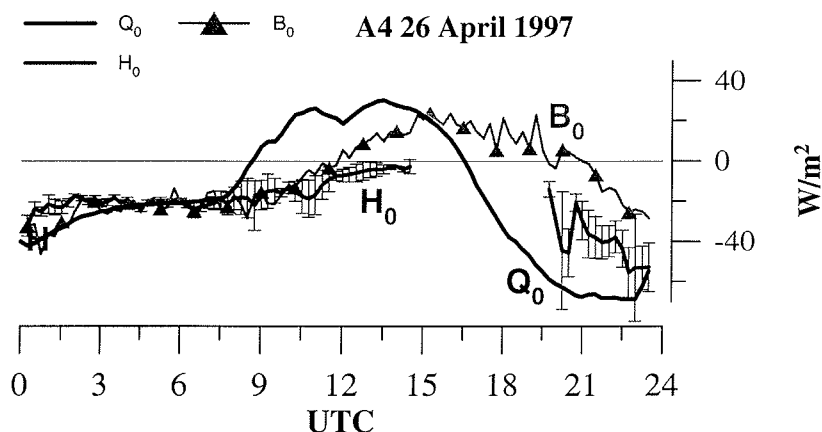


Fig. 8: As Figure 6b, but for 26 April (Res not displayed).

Abb. 8: Wie Abb. 6b, aber für den 26. April (Res nicht dargestellt).

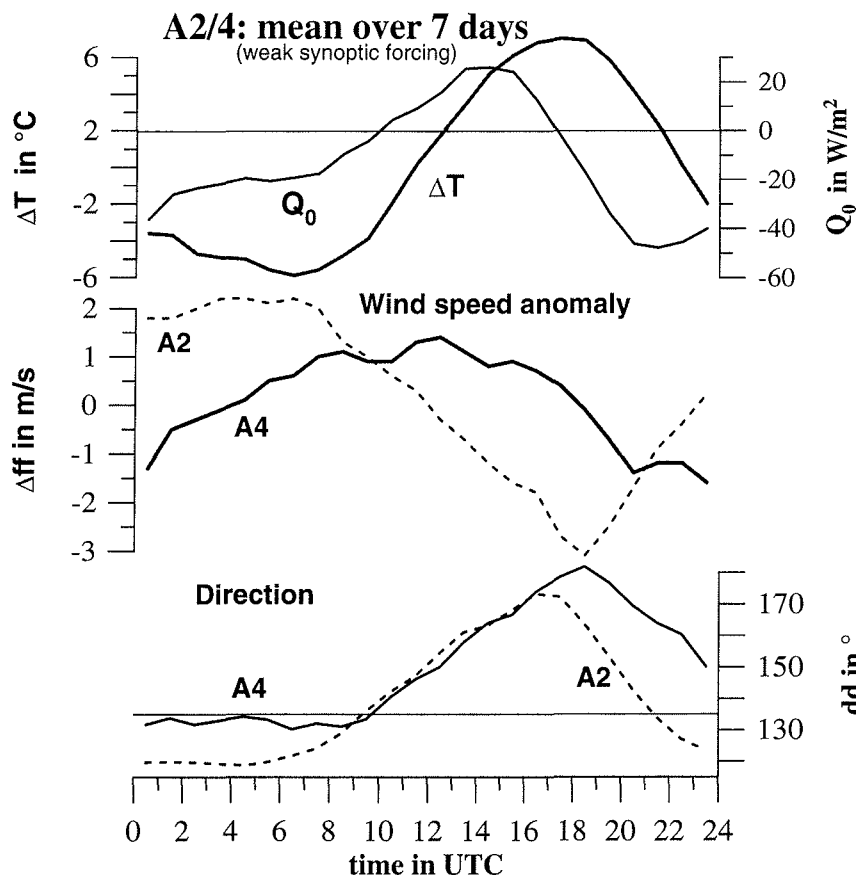


Fig. 9: Mean daily courses of selected quantities (1 h averages) at stations A2 (dashed lines) and A4 (solid lines) on the inland ice for a period with weak synoptic forcing (26 April to 2 May 1997). For temperature and wind speed, the anomaly from the low-pass filtered time series is shown (see text). The wind direction of 135° (35° and 45° relative to the local fall line for A2 and A4, respectively) is shown as a thin line.

Abb. 9: Mittlerer Tagesgang von ausgewählten Größen (1 h Mittel) an den Stationen A2 (gestrichelte Linien) und A4 (durchgezogene Linien) über dem Inlandeis für einen Zeitraum mit schwachem synoptischen Antrieb (26. April bis 2. Mai 1997). Für Temperatur und Windgeschwindigkeit werden Anomalien von den tiefpassgefilterten Zeitreihen dargestellt (s. Text). Die Windrichtung von 135° (35° und 45° relativ zur lokalen Falllinie für A2 bzw. A4) ist als dünne Linie eingezeichnet.

11. Data which did not pass the quality check according to the limits for convergence (taken as 3.0 for h) and the cost function (taken as 0.3 for J) are excluded (see Appendix II). In addition, the lower limit of u is set to 0.05 m/s, in order to exclude intermittent turbulence and weak wind conditions. Inconsistent profiles (gradient changes sign between different heights) are also discarded. Overall, only 46 % of the fluxes computed by the variational method are kept for A4. The stability parameter of the surface layer z/L is in the range of ± 0.1 for the majority of data points, which reflects that the dynamical production of turbulence by the katabatic wind is relatively strong. H_0 ranges between -100 and $+150$ $W m^{-2}$ with about 84 % of the values being inside the interval ± 50 $W m^{-2}$, and the error is smaller than 25 $W m^{-2}$ in general. As expected, u is largest for near-neutral stability, and reaches 0.6 m/s during strong katabatic winds. The error of u is smaller than 0.1 m/s.

The "classical" generation of the katabatic wind system is given by the cooling of the boundary layer caused by the vertical divergences of net radiation and sensible heat. The stability of the near-surface air depends on the radiative cooling of the surface, which in turn is connected to the wind speed and the associated sensible heat flux. This coupling between net radiation and sensible heat flux was already depicted in the discussion of individual days, and is shown in Figure 12 for the whole KABEG period. Although a correlation between negative H_0 and negative Q_0 can be seen, a large scatter is present. One main reason for this scatter is the phase lag between H_0 and Q_0 in the daily course. Firstly, the wind speed for the days of weak synoptic forcing (Fig. 9) has a

minimum during the evening, when the net radiation is already strongly negative. Secondly, a positive Q_0 cannot always destroy the stable stratification in the surface layer (negative H_0), as it is the case for the example of 22 April (Fig. 6b) and 26 April (Fig. 8). Both effects lead to a hysteresis for a sector with weak negative H_0 and a wide range of Q_0 values. The picture gets more unambiguous, if only daily means for conditions with $Q_0 < 0$ are taken into account. Q_0 and H_0 follow a much more linear relationship for these daily values, since most of the phase shift is lost by the averaging. In the average over the period 18 April to 16 May, Q_0 and H_0 had values of -14.0 and -7.6 $W m^{-2}$, respectively. But, these values represent not the real averages, since more daytime than nighttime fluxes are excluded by the quality control. For comparison, the average for the continuously measured net radiation for the whole period is -12 $W m^{-2}$ at A4 (the corresponding value at S has a value of 122 $W m^{-2}$).

For the quality check of the fluxes at S, less restrictive limits are chosen (10.0 for h , and 0.5 for J), otherwise the same criteria as for A4 are used for the selection of profiles. However, the restriction to the sectors with sufficient fetch leads to a strong reduction of the usable data. Figure 13 shows the comparison of measured eddy-correlation (HEC) and profile-derived (HSP) sensible heat at station S. Large deviations occur for stable situations and for large positive heat fluxes. The root mean square (RMS) difference for the positive branch is 25 $W m^{-2}$. Possible errors for the stable branch (instationarity, intermittency) have been mentioned in the previous Section. It should be noted that the systematic overestimation of the absolute value of the sensible heat flux

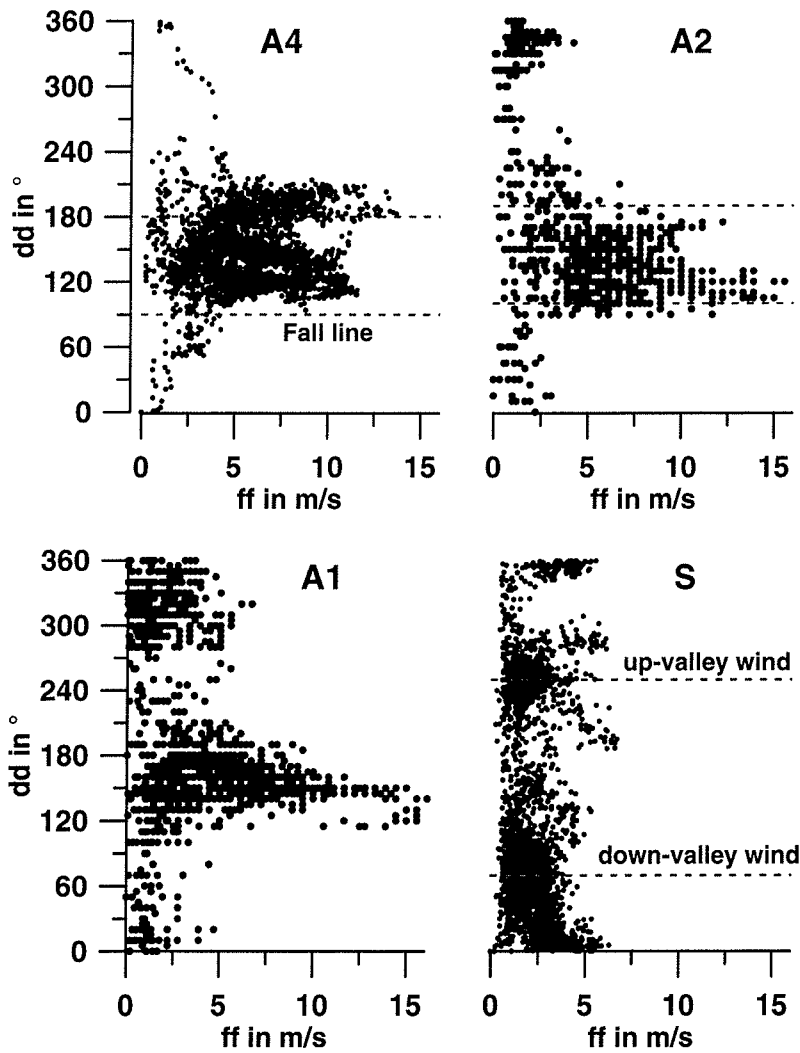


Fig. 10: Wind direction (dd) statistics as a function of wind speed (ff) at A4, A2, A1 and S. In the upper two panels, dashed lines mark the directions parallel and normal to the fall line, dashed lines in the lower right panel mark the directions parallel to the fjord valley axis.

Abb. 10: Statistik der Windrichtung (dd) als Funktion der Windgeschwindigkeit (ff) an A4, A2, A1 und S. Im oberen Teilbild markieren gestrichelte Linien die Windrichtungen parallel und normal zur lokalen Falllinie, im unteren rechten Teilbild die Windrichtungen parallel zur Achse des Fjord-Tals.

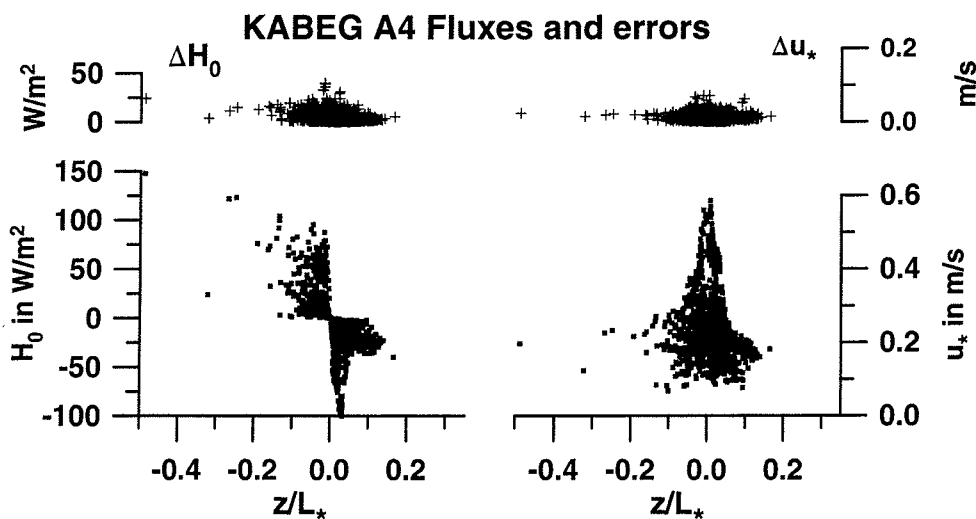


Fig. 11: Sensible heat flux (H_0) and surface layer velocity scale (u_*) as a function of the stability parameter z/L_* at A4 computed from the profile measurements for the whole measurement period. Upper panels show the errors of the variational method.

Abb. 11: Flussdichten sensibler Wärme (H_0) und Geschwindigkeitsskala der Prandtl-Schicht (u_*) als Funktion des Stabilitätsparameters z/L_* an A4 berechnet aus den Profilmessungen der gesamten Messperiode. Die oberen Teilbilder zeigen die Fehler aus der variationalen Methode.

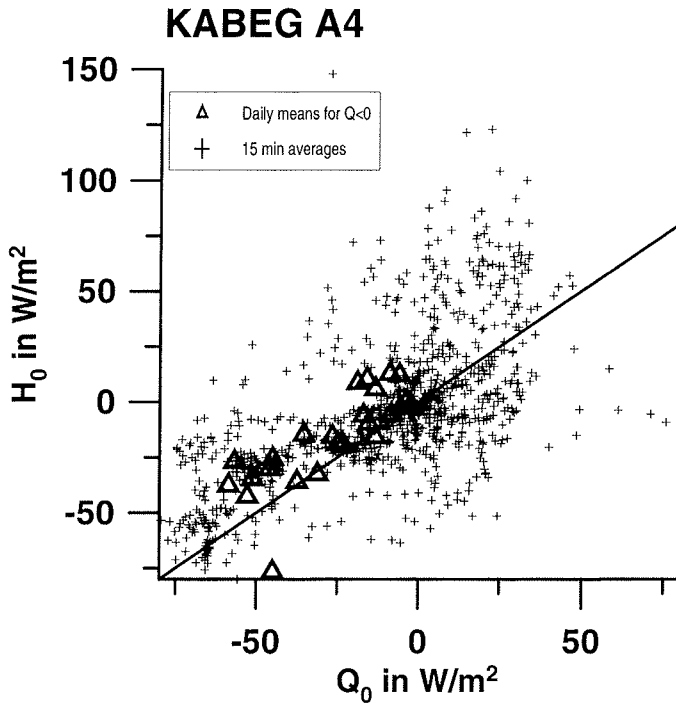


Fig. 12: Sensible heat flux (H_0) as a function of the net radiation (Q_0) at A4 for the whole measurement period. Crosses mark single values, open triangles mark daily averages for periods with $Q_0 < 0$.

Abb. 12: Flussdichte sensibler Wärme (H_0) als Funktion der Strahlungsbilanz (Q_0) an A4 für die gesamte Messperiode. Kreuze markieren Einzelwerte, offene Dreiecke stellen Tagesmittel für Zeiträume mit negativer Strahlungsbilanz ($Q_0 < 0$) dar.

for stable stratification by profile-derived fluxes was also found by FORRER (1999) for measurements over the ice sheet. The differences between HEC and HSP are generally much larger than the errors as computed by the variational method (not shown). This means that although the profiles are represented well by the MO similarity functions given by (I-8), they are not in complete agreement with the turbulent fluxes of the underlying surface, which may be caused by violations of the assumption of MOST (i.e. advection, instationarity, radiative heating).

Roughness lengths

Roughness lengths z_0 have not been used for the evaluation of the energy and momentum fluxes, but are also of interest for related studies using single-level measurements or model parameterizations. The data evaluation is performed according to HEINEMANN (1989), i.e. the selection of neutral profiles and the computation of z_0 by regression. Fig. 14 shows the results for A4. Neutral z_0 values show a large scatter for low wind speeds (low u_*) and a general increase with increasing u_* , with agrees well with the CHARNOCK (1955) relation:

$$z_0 = a \cdot \frac{u_*^2}{g}$$

taking $a = 0.016$. Visual observations showed that snow drift was present during strong wind situations, therefore explaining this behaviour of z_0 . The corresponding neutral drag coefficients C_{DN} for a reference height of 10 m show

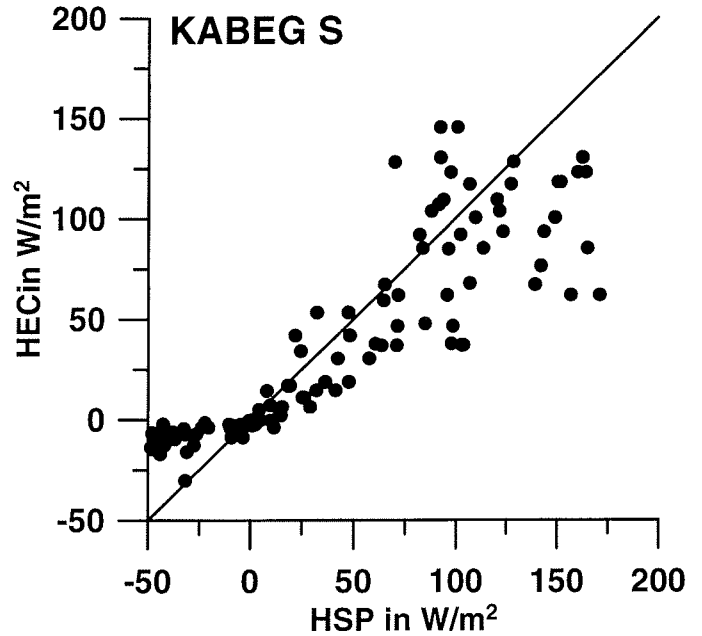


Fig. 13: Comparison of measured eddy-correlation (HEC) and profile-derived (HSP) sensible heat at station S. Only cases passing the quality tests are included (see text).

Abb.13: Vergleich von Flussdichten sensibler Wärme nach Eddy-Korrelationsmessungen (HEC) und Profilmessungen (HSP) an der Station S. Es gehen nur Werte ein, die den Qualitätstest passiert haben (s. Text).

values around 10^{-3} , but again a considerable scatter. The average of all z_0 values is 1.1×10^{-4} m. These results agree with those over flat Antarctic ice shelf surfaces, e.g. HEINEMANN (1989) and KÖNIG (1985).

Values for z_0 have also been computed for the tundra station with a vegetation height of about 0.5 m. Like for the evaluation of the turbulent fluxes, a fixed displacement height of 0.3 m was taken. The resulting z_0 values show very little scatter compared to A4 and are in the range of 1.5 to 3.5 cm with an average value of 2.3 cm (not shown).

SUMMARY AND CONCLUSIONS

Data of surface stations in the tundra area and over the ice sheet are evaluated for the KABEG period during April and May 1997. The wind measurements of the ice sheet stations show a pronounced daily cycle of the near-surface wind for almost all days indicating the nighttime development of the katabatic wind, which is found to be strongest close to the ice edge and shows a time lag of a few hours with respect to the net radiation. The daily course averaged over seven days with weak synoptic forcing yields a peak to peak amplitude of 5 m/s for the wind speed anomaly at station A2 close to the ice edge. The katabatic wind signal is most pronounced for the wind direction at all stations on the ice sheet, while the daily course and the maximum values of the wind speed are strongly influenced by the synoptic forcing. The katabatic wind dissipates quickly after crossing the ice edge for weak synoptic forcing, but a strong synoptic forcing supports the katabatic flow to extend about 10 km across the ice edge. Measurements in the Kangerlussuaq fjord valley (at a distance

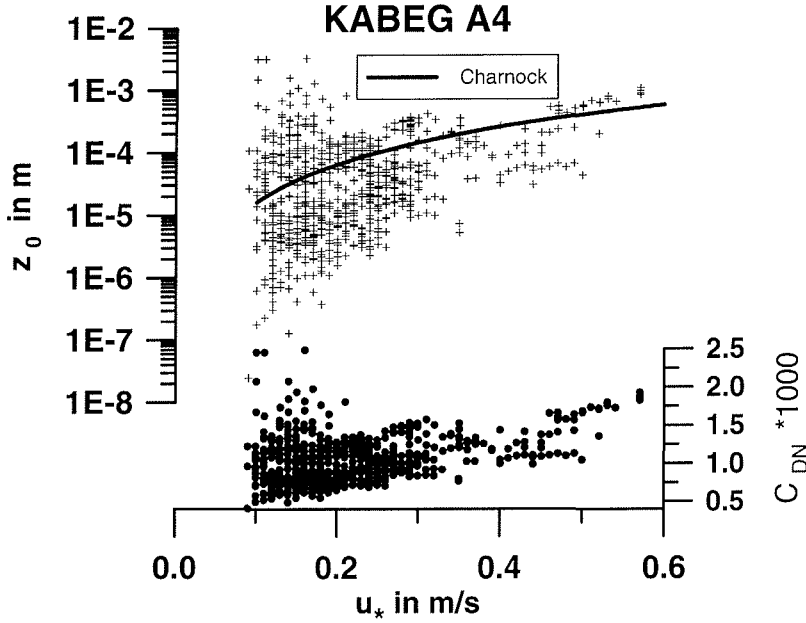


Fig. 14: Roughness length and drag coefficient (C_{DN} for 10 m) for neutral conditions as a function of u_* at A4 for the whole measurement period. The Charnock relation is also shown.

Abb. 14: Rauheitslängen und Widerstandskoeffizient (C_{DN} für 10 m) für neutrale Schichtung als Funktion von u_* an A4 für die gesamte Messperiode. Die Charnock-Relation wird ebenfalls gezeigt.

of about 20 km to the ice edge) show a weak down-valley wind during these situations.

Energy balance measurements have been evaluated for the fjord station S and for station A4 over the ice sheet (about 75 km from the ice edge). A variational approach is used to compute turbulent fluxes from profiles in the surface layer, since several reasons prohibited the application of the Bowen ratio method. The method is based on the MO similarity, whose conditions are not always fulfilled particularly for the tundra area. The comparison with eddy-correlation measurements shows that profile-derived sensible heat fluxes show the tendency to overestimate the absolute flux values for stable conditions over the tundra area. In contrast, the nighttime conditions over the ice sheet are typically associated with katabatic wind conditions, which lead to a sufficient shear generation of turbulence and quasi-stationary profiles. The energy loss by the net radiation over the ice sheet is compensated to a large extent by the turbulent flux of sensible heat during strong wind conditions. The determination of roughness lengths for neutral conditions yielded mean values of 2.3 cm and 1.1×10^{-4} m for the vegetated tundra area and the ice surface at A4, respectively. Roughness lengths over the ice sheet are in accordance with the CHARNOCK (1955) relation.

Accurate measurements of near-surface quantities and surface energy balance components over the Greenland ice sheet and in the tundra area are important for the validation of numerical models (e.g. KLEIN et al. 2001a,b) and as ground truth for measurements above the surface, such as remote sensing of the boundary layer over the ice sheet (e.g. MEESTERS et al. 1997) or aircraft-based measurements (e.g. HEINEMANN 1999). The knowledge of the processes of the air-snow exchange and their interaction with the atmospheric boundary layer, particularly the development of the katabatic wind system in the stable boundary layer, is also highly relevant for questions of climatic change (e.g. MEESTERS 1994). Special measurement campaigns like KABEG or GIMEX or the long-term AWS measurements of the PARCA program (STEFFEN et al. 1996) have yielded valuable datasets for model validations, which

may result in a better estimate of the energy and mass exchange of the Greenland and the Antarctic ice sheet.

APPENDIX I DESCRIPTION OF THE VARIATIONAL METHOD FOR THE COMPUTATION OF TURBULENT FLUXES

The variational approach follows the way outlined by XU & QUI (1997). The general idea is the minimization of a cost function J given by

$$J = \frac{1}{2} \sum_{k=2}^N \left\{ w_u (\Delta u_k - \Delta u_k^{obs})^2 + w_\theta (\Delta \theta_k - \Delta \theta_k^{obs})^2 + w_q (\Delta q_k - \Delta q_k^{obs})^2 \right\} + w_\delta \delta^2 \quad (I-1)$$

Δu_k , $\Delta \theta_k$ and Δq_k are the theoretical differences of wind speed, potential temperature and specific humidity, respectively, between the measuring heights z_k and the lowest level, and δ is the imbalance of the surface energy balance. Δu_k , $\Delta \theta_k$ and Δq_k are calculated using integrated MO similarity functions Ψ :

$$\Delta u_k = \Delta u(z_1, z_k, u_*, \theta_*, q_*, d) = \frac{u_*}{k} \left[\ln \frac{z_k - d}{z_1 - d} - \Psi_m \left(\frac{z_k - d}{L_*} \right) + \Psi_m \left(\frac{z_1 - d}{L_*} \right) \right] \quad (I-2a)$$

$$\Delta \theta_k = \Delta \theta(z_1, z_k, u_*, \theta_*, q_*, d) = \frac{\theta_*}{k} \left[\ln \frac{z_k - d}{z_1 - d} - \Psi_h \left(\frac{z_k - d}{L_*} \right) + \Psi_h \left(\frac{z_1 - d}{L_*} \right) \right] \quad (I-2b)$$

$$\Delta q_k = \Delta q(z_1, z_k, u_*, \theta_*, q_*, d) = \frac{q_*}{k} \left[\ln \frac{z_k - d}{z_1 - d} - \Psi_q \left(\frac{z_k - d}{L_*} \right) + \Psi_q \left(\frac{z_1 - d}{L_*} \right) \right] \quad (\text{I-2c})$$

The lowest measuring height is denoted by z_1 , (u_*, θ_*, q_*, d) is the unknown vector of surface layer scaling parameters and the displacement height. The imbalance of the surface energy balance

$$\delta = Q_0 - B_0 - H_0 - E_0 = Q_0 - B_0 + \rho c_p u_* \theta_* + \rho L u_* q_* \quad (\text{I-3})$$

can be added to the cost function as a boundary condition (Q_0 : net radiation, H_0 : turbulent flux of sensible heat, E_0 : turbulent flux of latent heat, B_0 : snow/soil heat flux). The w 's are weighting functions, which have been chosen according to the measurement errors of the respective quantities, and are used to make the cost function circumpolar, so that the applied minimization gets easier to the function's minimum. In that way every information available (first to third term in Equation (I-1) include the information given by the MO similarity theory, the fourth term includes the information of the energy balance of a surface) is used simultaneously.

The main problem for solving (I-1)-(I-2) is the adequate variation of the unknown quantities for finding the minimum of the cost function. This is done iteratively using a BFGS (Broyden-Fletcher-Goldfarb-Shanno) numerical method belonging to the class of Oren-Luenberger methods (OREN & LUENBERGER 1974, ÜBERHUBER 1995). An overview over these 'Quasi-Newton' methods is given in DENNIS and MORÉ (1977). The minimization requires the knowledge of the Hesse matrix \underline{H} :

$$H_{ij} = \frac{\partial^2 h}{\partial x_i \partial x_j} \quad \text{with} \quad h = |\bar{\nabla} J| = \sqrt{\sum_i \left(\frac{\partial J}{\partial x_i} \right)^2} \quad \text{and} \quad \bar{x} = (u_*, q_*, \theta_*) \quad (\text{I-4})$$

The minimum of h is found during the iteration process, starting with an initial guess of $u_* = u_0, \theta_* = \theta_0, q_* = 0$, and $\underline{H}_0 = \underline{1}$. The displacement height is set to a constant value for our data, the iteration vector is therefore reduced to three dimensions. By using this variational method, the search direction for a new value of \bar{x} at the iteration step n is calculated from \underline{H} and the gradient of h :

$$\bar{s}^n = \underline{H}^n \cdot \bar{g}^n; \bar{g}^n = \bar{\nabla} h^n \quad (\text{I-5})$$

The new value of \bar{x} for the iteration step $(n+1)$ is found by minimizing the line search problem:

$$\min_{\lambda \geq 0} \left\{ h(\bar{x}^n - \lambda \bar{s}^n) \right\} \quad \text{and} \quad \bar{x}^{n+1} = \bar{x}^n - \lambda \bar{s}^n \quad (\text{I-6})$$

using the minimization method of NOCEDAL (1980).

In order to avoid the explicit calculation of \underline{H} , the following recursion formula is used for an approximation of \underline{H} for the iteration step $(n+1)$:

$$\begin{aligned} \bar{p} &= \bar{x}^{n+1} - \bar{x}^n; \bar{r} = \bar{g}^{n+1} - \bar{g}^n \\ \underline{H}^{n+1} &= \underline{H}^n + \left(1 + \frac{\bar{r}^T \underline{H}^n \bar{r}}{\bar{p}^T \bar{r}} \right) \\ \frac{\bar{p} \bar{p}^T}{\bar{p}^T \bar{r}} &- \frac{1}{\bar{p}^T \bar{r}} (\bar{p} \bar{r}^T \underline{H}^n + \underline{H}^n \bar{r} \bar{p}^T) \end{aligned} \quad (\text{I-7})$$

The main advantage of this method is the fast convergence. In general, the minimum of h is found in M iterations (with M being the number of parameters on which the cost function depends), if h is a quadratic function and the minimization described in (I-6) is exact (NOCEDAL 1980, DENNIS & MORÉ 1977).

The MO similarity functions are taken from KAIMAL & FINNIGAN (1994) as:

$$\begin{aligned} \varphi_m &= \left(1 - 16 \frac{z-d}{L_*} \right)^{-\frac{1}{4}} \quad \text{and} \quad \varphi_h = \varphi_q = \varphi_m^2 \\ \text{for} \quad -2 &\leq \frac{z-d}{L_*} \leq 0 \end{aligned} \quad (\text{I-8})$$

$$\varphi_m = \varphi_h = \varphi_q = \left(1 + 5 \frac{z-d}{L_*} \right) \quad \text{for} \quad 0 \leq \frac{z-d}{L_*} \leq 1$$

As shown in Section 3, z/L_* values over the ice sheet were in the range of -0.5 to $+0.2$ with about 95 % of the values being inside the interval ± 0.1 , i.e. near-neutral conditions were present. For the tundra area, weak winds were prevailing and $(z-d)/L_*$ values between -0.8 and $+0.4$ were found.

APPENDIX II PERFORMANCE OF THE VARIATIONAL ANALYSIS FOR KABEG

For the evaluation of the KABEG data, the set of equations (I-1)-(I-3) was reduced. No use was made of the surface energy balance ($w_6 = 0$), since soil heat flux and humidity gradient measurements were not available or not reliable (see experiment section). For the same reasons, w_4 was set to zero over the ice sheet (at station S humidity measurements using psychrometers have been performed successfully only for a few days in May 1997). For the very smooth ice surface $d = 0$ was assumed, for the tundra station S the displacement height was set to $2/3$ of the vegetation height.

The weights $w_i = (\Delta y)^2$ have been chosen according to the measurement errors of the respective quantities, with Δy being the measurement error of wind speed (0.3 m/s), of temperature (0.2 K) and of humidity (0.1 g/kg), respectively. While the value of J is a measure of the closeness of the observed profiles to those of the MO similarity theory, h is a measure of

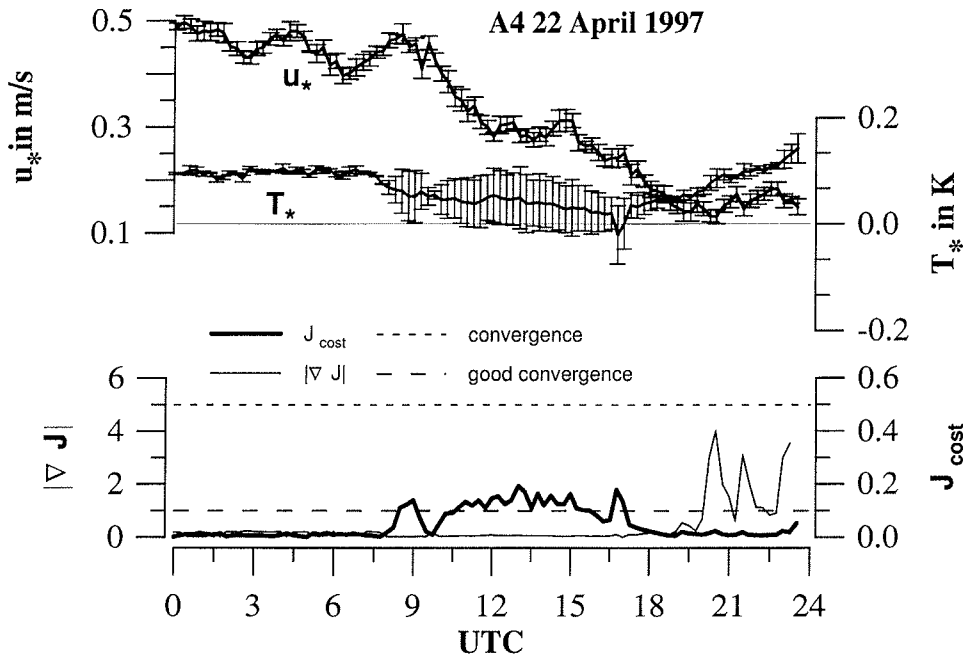


Fig. 15: Daily course of the surface layer velocity scale u_* and temperature scale T_* (upper panel, error bars calculated from the differences between the measured profiles and profiles according to MO similarity), the cost function J and the gradient function (lower panel) for 22 April at A4. For details see text.

Abb. 15: Tagesgang der Prandtl-Schicht-Skalen (oberes Teilbild) für Wind (u_*) und Temperatur (T_*) für den 22. April an A4. Die Fehlerbalken wurden aus den Differenzen zwischen gemessenen Profilen und den Profilen nach der MO-Ähnlichkeit berechnet. Die Kostenfunktion J und die Gradientenfunktion sind im unteren Teilbild dargestellt (Details s. Text).

the quality of the variational method in finding the minimum. The limit for reasonable convergence is set at 5.0 for J . Analogously, the agreement with MO can be regarded as good/reasonable, if the cost function itself has values lower than 0.1/0.5.

The variational analysis was applied to the measurements at A4 and S. Figures 15 and 16 show results for the strong wind case of 22 April 1997 (see result section). Since no humidity profile was measured, only the surface layer scaling parameters u_* and T_* are used for the minimization. In addition, the value of the cost function J and its gradient are shown. For the strong wind during the first half of 22 April at A4, relative high values for u_* and T_* are calculated. The error bars depict the standard deviations between the measured profile and profile according to MO similarity for wind and temperature, respectively. While these errors as well as the total cost function are very small until 8 UTC, an increase of these quantities is observed during daytime. This is mainly caused by larger deviations for the temperature profile. Although the temperature sensors were electrically ventilated, some influences of the radiation error during conditions of high insolation seem to be present. After 18 UTC errors and the cost function decrease again, but now the gradient of the cost function indicates that the convergence for finding the minimum is worse than before. But overall, the variational method yields very satisfying results for the evaluation of the profile measurements at A4.

The situation is quite different for the tundra station S (Fig. 16). While the errors for T_* are relatively small in general, u_* shows large uncertainties (deviations from the theoretical profiles). Although the surface roughness of the tundra area is much higher compared to the ice sheet, u_* values are much smaller because of the low wind speeds in the fjord valley. The minimization method works well for almost all profiles, but the values for the cost function exceed the acceptable limits for many profiles.

In contrast to the overall good quality of the variational method at A4 for 22 April, the evaluation for the case with

weak synoptic forcing on 26 April (see result section) shows some problems for this method (Fig. 17). While the results are of good quality between 00 and 14 UTC, relatively large values of J and severe problems for finding the minimum can be detected during the rest of the day, particularly during the cooling phase during the afternoon associated with wind speeds around 2 m/s (see result section).

ACKNOWLEDGMENTS

KABEG was supported by the German Federal Ministry of Education, Science, Research and Technology under grant BMBF-03PL020F. We would like to thank all people at MIUB, who helped in the preparation and organization of KABEG, in particular C. Drüe, who participated in the field measurements. The authors are also grateful to the DMI (Copenhagen and Kangerlussuaq) and the Institute of Marine and Atmospheric Research University Utrecht (IMAU) for support.

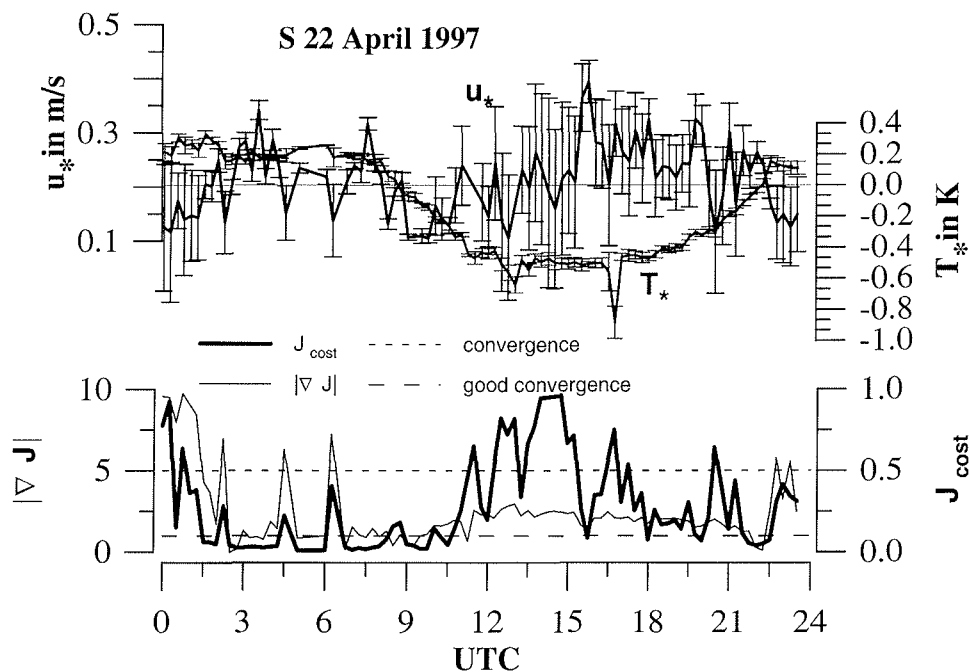


Fig. 16: As Figure 15, but for 22 April at S.

Abb. 16: Wie Abb. 15, aber für den 22. April an S.

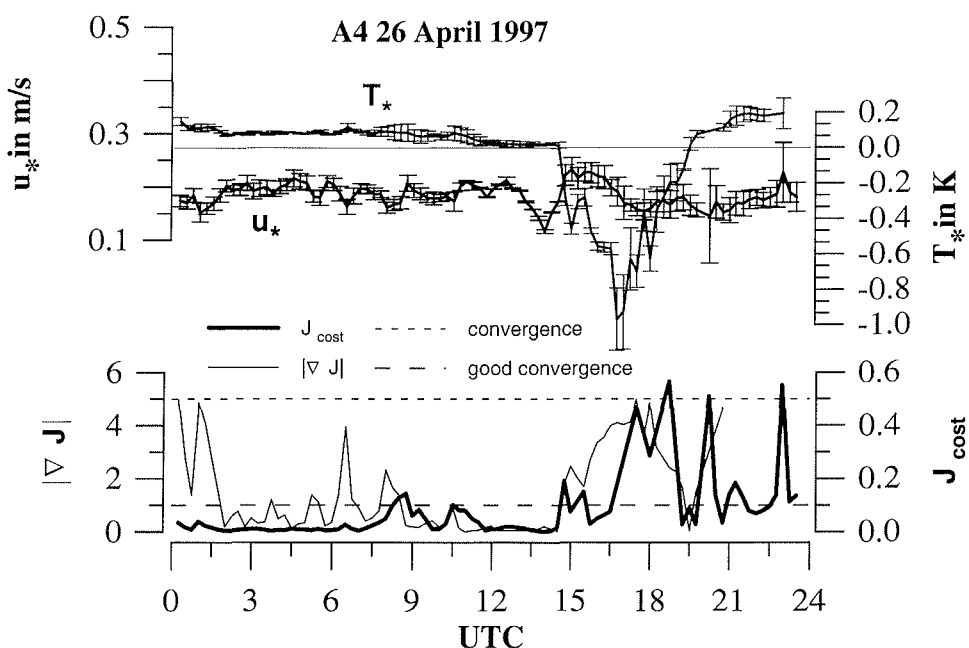


Fig. 17: As Figure 15, but for 26 April at A4.

Abb. 17: Wie 15, aber für den 26. April an A4.

References

- Bowen, I.S. (1926): The ratio of heat losses by conduction and by evaporation from any water surface.- *Phys. Rev.* 27: 779-787.
- Charnock, H. (1955): Wind stress on a water surface.- *Quart. J. R. Met. Soc.* 81: 639-640.
- Dennis, J.E. & Moré, J.J. (1977): Quasi-Newton methods, motivation and theory.- *SIAM Rev.* 19: 46-89.
- Ekholm, S. (1996): A full coverage, high-resolution, topographic model of Greenland computed from a variety of digital elevation data.- *J. Geophys. Res.* 101: 21961-21972.
- Foken, T. & Wichura, B. (1996): Tools for quality assessment of surface-based flux measurements.- *Agr. For. Meteorol.* 78: 83-105.
- Forrer, J. & Rotach, M.W. (1997): On the structure in the stable boundary layer over the Greenland ice sheet.- *Boundary Layer Meteorol.* 85: 111-136.
- Forrer, J. (1999): The structure and turbulence characteristics of the stable boundary layer over the Greenland ice sheet.- *Zürcher Klimaschriften* 75, ETH Zürich, 132 pp.

- Heinemann, G. (1989): Über die Rauigkeitslänge Z_0 der Schneeoberfläche des Filchner-Ronne-Schelfeises.- *Polarforschung* 59: 17-24.
- Heinemann, G. & Rose, L. (1990): Surface energy balance, parameterizations of boundary layer heights and the application of resistance laws near an Antarctic ice shelf front.- *Boundary Layer Meteorol.* 51: 123-158.
- Heinemann, G. (1998): Katabatic wind and boundary layer front experiment around Greenland (KABEG) field phase report.- *Reports Polar Res.* 269: 1-93.
- Heinemann, G. (1999): The KABEG'97 field experiment: An aircraft-based study of the katabatic wind dynamics over the Greenlandic ice sheet.- *Boundary Layer Meteorol.* 93: 75-116.
- Kaimal, J.C. & Finnigan, J.J. (1994): *Atmospheric Boundary Layer Flows. Their Structure and Measurement.* - Oxford University Press, Oxford, 289 pp.
- Klein, T., Heinemann, G., Bromwich, D.H., Cassano, J.J. & K.M. Hines (2001a): Mesoscale modeling of katabatic winds over Greenland and comparisons with AWS and aircraft data.- *Meteor. Atmosph. Phys.* 78: 115-132.

- Klein, T., Heinemann, G. & Gross, P.* (2001b): Simulation of the katabatic flow near the Greenland ice margin using a high-resolution nonhydrostatic model.- *Meteorol. Zeitschrift* N.F. 10: 331-339.
- König, G.* (1985): Roughness length of an Antarctic ice shelf.- *Polarforschung* 55: 27-32.
- Ma, J. & Daggupati, S.M.* (2000): Using all observed information in a variational approach to measuring Zom and Zot.- *J. Appl. Meteorol.* 39: 1391-1401.
- Meesters, A.* (1994): Dependence of the energy balance of the Greenland ice sheet on climatic change: Influence of the katabatic wind and tundra.- *Quart. J. R. Meteorol. Soc.* 120: 491-517.
- Meesters, A., Bink, N., Henneken, E., Vugts, H. & Cannemeijer, F.* (1997): Katabatic wind profiles over the Greenland ice sheet: observation and modelling.- *Boundary Layer Meteorol.* 85: 475-496.
- Nocedal, J.* (1980): Updating quasi-Newton matrices with limited storage.- *Mathematics of Computation* 35: 773-782.
- Oerlemans, J. & Vugts, H.* (1993): A meteorological experiment in the ablation zone of the Greenland ice sheet.- *Bull. Am. Meteorol. Soc.* 74: 355-365.
- Ohmura, A., Wild, M. & Bengtsson, L.* (1996): A possible change in mass balance of Greenland and Antarctic ice sheets in the coming century.- *J. Climate* 9: 2124-2135.
- Oren, S. S. & Luenberger, D.G.* (1974): Self-scaling variable metric algorithms I: Criteria and sufficient conditions for scaling a class of algorithms.- *Man. Sci.* 20: 845-862.
- Putnins, P.* (1970): The climate of Greenland.- In: S. ORVIG (ed.), *Climates of the polar regions*, *World Survey of Climatology* 14: 3-113.
- Rasmussen, L.* (1989): Greenland winds and satellite imagery.- *Vejret, Danish Meteorol. Soc.*: 32-37.
- Steffen, K., Box, J.E. & Abdalati, W.* (1996): Greenland Climate Network: GC-Net.- In: S.C. COLBECK (ed.), *CRREL 97-26 Special Report on Glaciers, Ice Sheets and Volcanoes*, 98-113.
- Svensson, K.* (1997): Aufbau einer Anlage für Turbulenzmessungen nach der Eddy-Korrelationsmethode.- *Diploma Thesis, Meteorol. Inst. Univ. Bonn*, 94 pp.
- Überhuber, C.* (1995): *Computer-Numerik 2.* - Springer Verlag Berlin, Heidelberg, 515 pp.
- Xu, Q. & Qui, C.-J.* (1997): A variational method for computing surface heat fluxes from ARM surface energy and radiation balance systems.- *J. Appl. Meteorol.* 36: 3-11.